Quality-guided orientation unwrapping for fringe direction estimation

Haixia Wang and Qian Kemao*

School of Computer Engineering, Nanyang Technological University, Singapore, 639798

*Corresponding author: mkmqian@ntu.edu.sg

Received 29 June 2011; revised 5 September 2011; accepted 5 September 2011; posted 7 September 2011 (Doc. ID 150016); published 24 January 2012

Fringe patterns produced by various optical interferometric techniques encode information such as shape, deformation, and refractive index. Denoising and demodulation are two important procedures to retrieve information from a single closed fringe pattern. Various existing denoising and demodulation techniques require fringe direction/orientation during the processing. Fringe orientation is often easier to obtain but fringe direction is needed in some demodulation techniques. A quality-guided orientation unwrapping scheme is proposed to estimate direction from orientation. Two techniques, one based on windowed Fourier ridges and the other based on fringe gradient, are proposed for the quality-guided orientation unwrapping scheme. The direction qualities are compared for both simulated and experimental fringe patterns. Their application to demodulation technique is also given.

OCIS codes: 100.2000, 100.2650, 100.2960.

1. Introduction

Optical interferometric techniques have been widely used for precision measurement. Fringe patterns are the outputs of these techniques and can be represented as

$$f(x,y) = b(x,y)\cos[\varphi(x,y)], \tag{1}$$

where (x,y) is the pixel coordinate and $f(x,y)$, $b(x,y)$, and $\varphi(x,y)$ are the recorded fringe intensity, fringe amplitude, and phase distribution, respectively [1]. The background intensity is not included in the fringe pattern model in Eq. (1) for convenience and it can be removed from real fringe patterns by techniques such as low pass filtering [1]. The information to be measured is often related to the phase. The process of retrieving phase from a single fringe pattern is called fringe pattern demodulation. The demodulation process may fail due to the noise presented in the fringe pattern, and denoising becomes necessary. Fringe pattern denoising and demodulation are thus two important aspects of processing a single fringe pattern. Fringe direction/orientation is an essential part of many existing denoising [2–5] and demodulation techniques [6–10]. Reliable direction/orientation estimation technique is of interest. Since orientation estimation techniques have been well established, this paper focuses on direction estimation.

As a preparation, fringe direction and fringe orientation are defined and their relationship is formulated. The fringe *direction* $\beta(x,y)$ is defined to be perpendicular to the gradient of the phase as follows [11],

$$[\cos\beta(x,y), \sin\beta(x,y)]\nabla\varphi(x,y) = 0, \tag{2}$$

where $\nabla\varphi(x,y) = [\varphi_x(x,y), \varphi_y(x,y)]^T$; $\varphi_x(x,y)$ and $\varphi_y(x,y)$ are derivatives of $\varphi(x,y)$ along x and y directions, respectively; and T denotes the transpose of a vector. The direction is then calculated as

$$\beta(x,y) = \arctan 2[-\varphi_x(x,y), \varphi_y(x,y)], \tag{3}$$

where $\arctan 2(y,x)$ is a four-quadrant arctangent function where the quadrant of the result is

1559-128X/12/040413-09$15.00/0

determined by the signs of both variables. It is obvious that $\beta(x,y) \in (-\pi,\pi]$ and thus modulo 2π. However, the phase derivatives in Eq. (3), $\varphi_x(x,y)$, and $\varphi_y(x,y)$ are usually unknown before fringe pattern demodulation.

Assuming that $b(x,y)$ is locally constant, according to Eq. (1), the fringe intensity gradient is

$$\begin{aligned}\nabla f(x,y) &= [f_x(x,y), f_y(x,y)]^T \\ &= -b(x,y)\sin[\varphi(x,y)][\varphi_x(x,y), \varphi_y(x,y)]^T, \quad (4)\end{aligned}$$

which suggests the possibility of estimating the direction from $\nabla f(x,y)$. However, a fringe pattern with $[\varphi(x,y),\varphi_x(x,y),\varphi_y(x,y)]$ or $[-\varphi(x,y),-\varphi_x(x,y),-\varphi_y(x,y)]$ has the same $\nabla f(x,y)$. Although they should have different directions according to Eq. (3), they cannot be differentiated by $\nabla f(x,y)$. In fact, only the fringe orientation $\theta(x,y)$, which is the fringe direction restricted into a range of $(-\pi/2,\pi/2]$, can be obtained from $\nabla f(x,y)$ as

$$\theta(x,y) = \arctan[-f_x(x,y)/f_y(x,y)]. \quad (5)$$

The orientation is modulo π. The detailed definition of orientation and direction can be found in [12]. There are many fringe orientation estimation techniques using fringe intensity, including the gradient-based technique [11], the plane-fit technique [2], the combined plane-fit and gradient-based technique [13], the 2D energy operator technique [14], and the accumulated differences technique [15]. Note that the Fourier transform based technique [16] estimates the orientation based on information in frequency domain instead of spatial domain. However, this technique requires complex pre- and post-processing of the fringe pattern and also produces modulo π fringe orientation.

The conversion from direction $\beta(x,y) \in (-\pi,\pi]$ to orientation $\theta(x,y) \in (-\pi/2,\pi/2]$ can be stated as

$$\theta(x,y) = \begin{cases} \beta(x,y) & -\pi/2 < \beta(x,y) \le \pi/2 \\ M_{2\pi}[\beta(x,y)+\pi] & \text{else} \end{cases}, \quad (6)$$

where $M_{2\pi}(\cdot)$ denotes the modulo 2π operation that adds or subtracts 2π so that the output is within the range of $(-\pi,\pi]$. On the contrary, the conversion from orientation to direction is more useful but also more challenging. Marroquin *et al.* minimize a quadratic energy function to determine the possibility of adding π to the orientation [6]. Quiroga *et al.* compute the fringe direction by phase unwrapping with a regularized phase tracking technique based on the fringe orientation information [17]. Its performance is affected by noise and scanning strategy [18,19]. The optimization processes used in both techniques [6,17] are computational costly. Siddiolo *et al.* unwrap the fringe orientation by classifying the gradient vector trends [10], where fringe denoising is needed before the unwrapping to obtain reliable gradient vectors.

As has been noticed by some researchers, conversion from direction to orientation "wraps" an angle from $(-\pi,\pi]$ to $(-\pi/2,\pi/2]$ by adding or subtracting π, while conversion from orientation to direction "unwraps" the angle from $(-\pi/2,\pi/2]$ to $(-\pi,\pi]$ also by adding or subtracting π. They are similar to the often encountered phase wrapping and unwrapping problems [20]. In this paper, a quality-guided orientation unwrapping scheme, similar to the quality-guided phase unwrapping, is proposed. It includes a simple but general orientation unwrapping criterion of how to add or subtract π, and a quality-guided strategy to avoid low orientation quality points and make the unwrapping successful.

Further, under the proposed quality-guided orientation unwrapping scheme, two practical techniques are proposed. The first technique is based on windowed Fourier ridges (WFR) [21,22]. The WFR estimates local frequencies from which the orientation can be calculated. These local frequencies can also be used to characterize the fringe density as the quality map to guide the orientation unwrapping. This technique provides directions with high accuracy especially for noisy fringe patterns, at a cost of long computing time. The second technique uses any existing techniques to estimate orientation. The gradient information is used to measure the density and to guide the orientation unwrapping. Comparatively, this unwrapping process is much faster. Experiments are carried out to verify the proposed techniques for simulated and experimental fringe patterns. Finally, as an example, the obtained directions are utilized for phase extraction from a single closed fringe pattern through a spiral phase quadrature (SPQ) transform [7,8].

The rest of the paper is organized as follows. The proposed quality-guided orientation unwrapping scheme is introduced in Section 2; the WFR-based orientation unwrapping is presented in Section 3; the gradient-based orientation unwrapping is presented in Section 4; the performances of the proposed techniques are compared and discussed in Section 5; the paper is concluded in Section 6.

2. Quality-Guided Orientation Unwrapping Scheme

The proposed quality-guided orientation unwrapping scheme consists of a criterion of how to add or subtract π to unwrap the orientation and a strategy of how to guide the unwrapping by a proper path.

The relationship between modulo π fringe orientation and modulo 2π fringe direction in one dimension is shown in Fig. 1 for illustration, where the solid line is the modulo 2π fringe direction while the dash line is the modulo π fringe orientation. Three conditions are encountered. First, for pixels between A and B, the orientation is continuous and no processing is required. Second, a jump of π occurs at pixel B, which requires an angle of π to be added to unwrap the orientation. The pixels between B and C are unwrapped in the same way. Third, for pixel C, an angle of π should be subtracted rather than added in order to keep

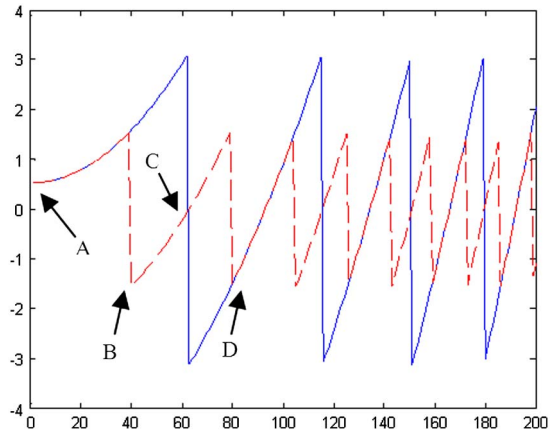

Fig. 1. (Color online) Orientation and direction.

the unwrapped value within the range of $(-\pi, \pi]$. The pixels between C and D are processed in the same way. All remaining pixels can be similarly unwrapped. The operations for second and third conditions can be unified by using the operation of $M_{2\pi}[\theta(x,y)+\pi]$.

In practice, to take the noise influence into account, a jump is identified if the orientation of the current pixel, $\theta(x,y)$, is different from the orientation of its adjacent and unwrapped neighbor, $\theta(x_0,y_0)$, by more than $\pi/2$. Consequently, two orientation vectors, $\{\cos[\theta(x,y)], \sin[\theta(x,y)]\}^T$ and $\{\cos[\theta_0(x,y)], \sin[\theta_0(x,y)]\}^T$, have a negative dot product. This leads to the following simple criterion for orientation unwrapping,

$$\beta(x,y) = \begin{cases} \theta(x,y) & \cos[\theta(x,y)]\cos[\theta(x_0,y_0)] + \sin[\theta(x,y)]\sin[\theta(x_0,y_0)] \geq 0 \\ M_{2\pi}[\theta(x,y)+\pi] & \text{else} \end{cases}. \quad (7)$$

However, if a pixel has the phase derivatives or local frequencies $[\varphi_x(x,y), \varphi_y(x,y)]^T$ close to zero, its direction is actually undetermined as Eq. (3) states. This is also true for its orientation as $[f_x(x,y), f_y(x,y)]^T$ is also small. The orientation unwrapping through these points can cause errors, and these errors are carried into all the pixels unwrapped afterwards. The unwrapping path is therefore important to avoid passing through low frequency pixels. A quality map indicating the frequency distribution, i.e., fringe density, can be used to guide the processing path to make the orientation unwrapping successful. This is the guiding strategy to be used.

With the above unwrapping criterion and guiding strategy, the quality-guided orientation unwrapping is summarized below and two specific techniques using this scheme will be introduced in next two sections,

Step 1: choose a pixel (x_0,y_0) with the highest quality as the seed pixel and use its orientation as its direction; push the seed pixel into an unwrapping register;

Step 2: select the pixel with the highest quality in the unwrapping register;

Step 3: unwrap the orientations of its four adjacent pixels based on Eq. (7), if they have not been processed; push the unwrapped pixels into the register;

Step 4: repeat steps 2 and 3 until all pixels are processed.

3. Windowed Fourier Ridges Based Orientation Unwrapping

To facilitate the quality-guided orientation unwrapping scheme for fringe direction estimation, an orientation map and a density map are required. The WFR technique [21,22] is able to provide both maps and thus proposed as our first technique for quality-guided orientation unwrapping. The WFR is a fringe pattern analysis technique based on windowed Fourier transform. It estimates the phase and local frequencies from a single fringe pattern with high tolerance to noise. Given a fringe pattern $f(x,y)$, its windowed Fourier transform is

$$Sf(u,v;\xi,\eta) = \int_{-\infty}^{\infty}\int_{-\infty}^{\infty} f(x,y) g^*_{u,v;\xi,\eta}(x,y)\mathrm{d}x\mathrm{d}y, \quad (8)$$

where $Sf(u,v;\xi,\eta)$ is the windowed Fourier spectrum; the symbol $*$ denotes the conjugate of a complex number; $g_{u,v;\xi,\eta}(x,y)$ is the windowed Fourier element defined as

$$g_{u,v;\xi,\eta}(x,y) = g(x-u,y-v)\exp(j\xi x + j\eta y); \quad (9)$$

(x,y) and (u,v) are used as spatial coordinates, while (ξ,η) is used as frequency coordinate. The spatial extension of the windowed Fourier transform is limited by the window function $g(x-u,y-v)$, where Gaussian window is used in this paper [22]. Different values of (ξ,η) in $g_{u,v;\xi,\eta}(x,y)$ yield different $Sf(u,v;\xi,\eta)$. The (ξ,η) maximizing $|Sf(u,v;\xi,\eta)|$, i.e., at the ridge of $|Sf(u,v;\xi,\eta)|$, is considered as the local frequencies at (u,v), which is formulated as [21,22]

$$[\omega_x(u,v), \omega_y(u,v)] = \arg\max_{\xi,\eta} |Sf(u,v;\xi,\eta)|, \quad (10)$$

where $\omega_x(u,v)$ and $\omega_y(u,v)$ denote the local frequencies at (u,v) along x and y, respectively. The phase

information can be further estimated based on the local frequencies.

According to the definition [21,22], $[\omega_x(x,y), \omega_y(x,y)] = [\varphi_x(x,y), \varphi_y(x,y)]$. However, when the WFR is applied to a single closed fringe pattern, the estimated local frequencies could be either $[-\omega_x(x,y), -\omega_y(x,y)]$ or $[\omega_x(x,y), \omega_y(x,y)]$, which is called the sign ambiguity problem [21–23]. Because of this ambiguity, only the fringe orientation can be estimated from the local frequencies as

$$\theta_{\mathrm{WFR}}(x,y) = \arctan[-\omega_x(x,y)/\omega_y(x,y)]. \quad (11)$$

Meanwhile, the total local frequency (TLF) is defined and computed as

$$D_{\mathrm{WFR}}(x,y) = \omega_{\mathrm{TLF}}(x,y) = \sqrt{\omega_x^2(x,y) + \omega_y^2(x,y)}. \quad (12)$$

The TLF indicates the fringe density distribution and can be used as the quality map. Having the fringe orientation from Eq. (11) and the quality map from Eq. (12), the fringe direction is obtained according to the quality-guided orientation unwrapping scheme in Section 2.

The estimation of $\omega_x(x,y)$ and $\omega_y(x,y)$ in the WFR, which is realized by exhaustive searching, is computational heavy. The computation time can be saved by restricting the searching range of ξ and η to $[\xi,\eta] \in [\xi_l,\xi_h] \times [\eta_l,\eta_h]$, which is a frequency band estimated through the fringe density or from Fourier spectrum of the fringe pattern [21,22].

However, the following problems inherent in the WFR are encountered, which subsequently affect the accuracy of fringe direction: (i) In the current WFR, $[\omega_x(x,y), \omega_y(x,y)]$ is exhaustively searched, which causes staircase local frequencies; (ii) $[\omega_x(x,y), \omega_y(x,y)]$ is not accurate in low frequency regions of a fringe pattern [21,22].

Gaussian filtering [24] solves both problems. After the fringe orientation has been unwrapped and the fringe direction has been obtained, a new local frequency field is constructed as $\{-\omega_{\mathrm{TLF}}(x,y)\sin[\beta(x,y)], \omega_{\mathrm{TLF}}(x,y)\cos[\beta(x,y)]\}$, which does not have the sign ambiguity problem. This field is separated into high frequency regions and low frequency regions by thresholding $\omega_{\mathrm{TLF}}(x,y)$ with a typical value of 0.1. In the high frequency regions, a narrow Gaussian window with a small kernel size σ_H is used to slightly smooth the staircases of local frequencies; in the low frequency regions, a wide Gaussian window with a large kernel size σ_L is used to recover the local frequencies from surrounding pixels. Two results are then combined and used to re-estimate the fringe direction using Eq. (3). Since the WFR is computationally intensive, this orientation unwrapping technique is not fast although the accuracy is often high.

4. Gradient-Based Orientation Unwrapping

The second technique proposed for quality-guided orientation unwrapping aims at faster speed. Since various techniques have been proposed for fringe pattern orientation estimation [2,11,13–16], they can be directly used. The gradient-based orientation estimation technique [11] is chosen for its easier implementation and better performance than existing techniques in [13,15] according to our comparisons. The orientation is estimated as follows:

$$\theta_{\mathrm{GRA}}(x,y) = \frac{1}{2}\arctan 2\Big\{-\sum_{u=x-\varepsilon}^{x+\varepsilon}\sum_{v=y-\varepsilon}^{y+\varepsilon} 2f_{x\sigma}(u,v)f_{y\sigma}(u,v), \sum_{u=x-\varepsilon}^{x+\varepsilon}\sum_{v=y-\varepsilon}^{y+\varepsilon}[f_{y\sigma}^2(u,v) - f_{x\sigma}^2(u,v)]\Big\}, \quad (13)$$

where ε is the averaging window size; $\nabla f_\sigma = [f_{x\sigma}, f_{y\sigma}]^T$ is used instead of ∇f, indicating that the fringe pattern undergoes a Gaussian filtering with a kernel size of σ before the gradient is calculated so that the gradient calculation will be more robust to noise.

Having obtained the orientation, the remaining task is to find a quality map representing the density information of the fringe pattern. According to Eq. (4),

$$|\nabla f(x,y)| = b(x,y)|\sin[\varphi(x,y)]|\omega_{\mathrm{TLF}}(x,y), \quad (14)$$

which is proportional to the total local frequency $\omega_{\mathrm{TLF}}(x,y)$ at each pixel, but it is "modulated" by $b(x,y)$ and $|\sin[\varphi(x,y)]|$. Unlike $b(x,y)$ which is often nearly a constant, the term $|\sin[\varphi(x,y)]|$ varies from 0 to 1, which distorts the TLF. To solve this problem, a Gaussian filter K_ρ with kernel size of ρ is used to smooth the gradient as

$$D_{\mathrm{GRA}} = K_\rho \otimes |\nabla f_\sigma(x,y)|, \quad (15)$$

where the symbol $\otimes$ denotes a convolution operator. Note that ∇f_σ is used for the same reason as Eq. (13). Thus, the kernel σ smooths the fringe pattern while the kernel ρ smooths the gradient field. In high frequency regions, $|\sin[\varphi(x,y)]|$ is fast varying and is flattened after being smoothed by K_ρ so that it does not distort the TLF much; in low frequency regions, $|\sin[\varphi(x,y)]|$ does not affect much since the TLF is already very low. The structure tensor has also been used for local density evaluation [25–27]. It is very similar to D_{GRA} both theoretically as well as in our experiments and can also be adopted as a quality measure in the quality-guided orientation unwrapping scheme.

Having an orientation map from Eq. (13) and a quality map from Eq. (15), the fringe direction can be obtained based on the quality-guided orientation unwrapping scheme in Section 2.

5. Comparisons and Discussions

In this section, the feasibility of the WFR based orientation unwrapping and the gradient-based orientation unwrapping are verified by applying

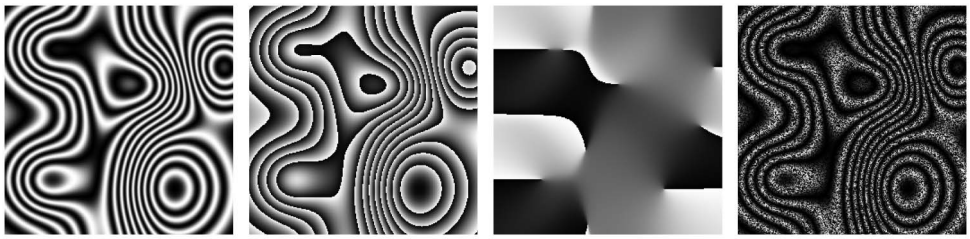

Fig. 2. Simulated fringe pattern. (a) Noiseless fringe pattern; (b) wrapped phase; (c) theoretical direction; (d) fringe pattern with speckle noise.

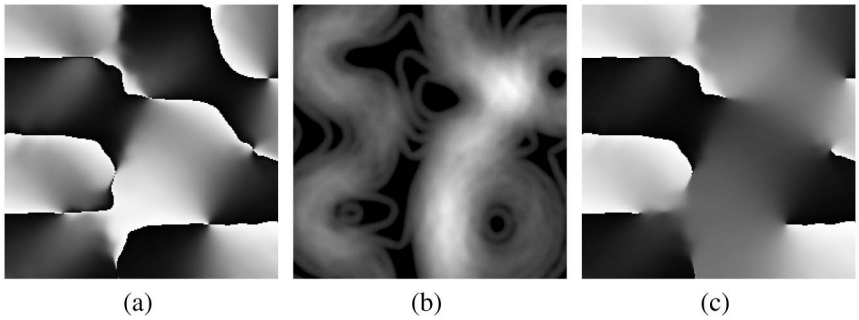

Fig. 3. WFR-based orientation unwrapping of Fig. 2(d). (a) Orientation θ_{WFR}; (b) density D_{WFR}; (c) direction β_{WFR}.

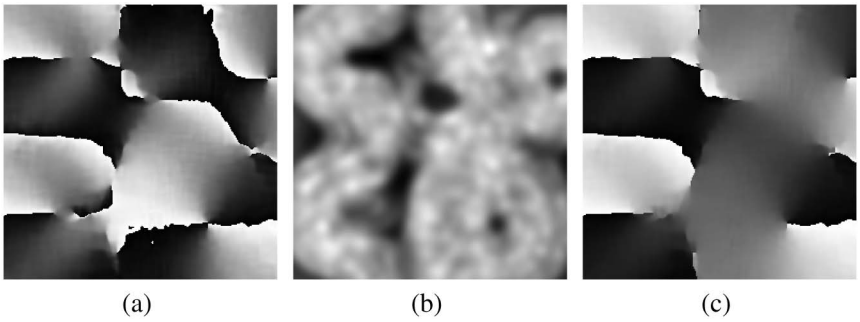

Fig. 4. Gradient-based orientation unwrapping of Fig. 2(d). (a) Orientation θ_{GRA}; (b) density D_{GRA}; (c) direction β_{GRA}.

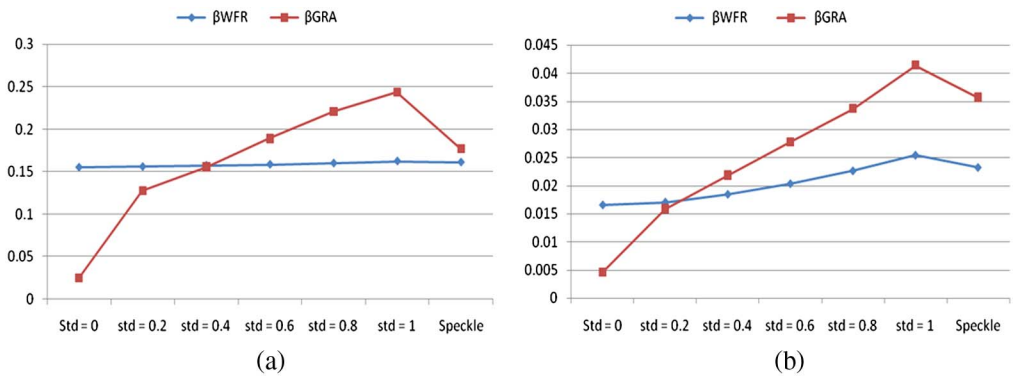

Fig. 5. (Color online) Direction error plots. (a) Error plots of direction results in low frequency regions; (b) error plots of direction results in high frequency regions.

them to simulated and experimental fringe patterns. The directions from the WFR-based and gradient-based orientation unwrapping are denoted as β_{WFR} and β_{GRA}, respectively. The accuracies of β_{WFR} and β_{GRA} for the simulated fringe pattern will be quantitatively evaluated by comparing them with

(a) (b) (c)

Fig. 6. Demodulation results of Fig. 2(d). (a) Phase obtained using β_T; (b) phase obtained using β_{WFR}; (c) phase obtained using β_{GRA}.

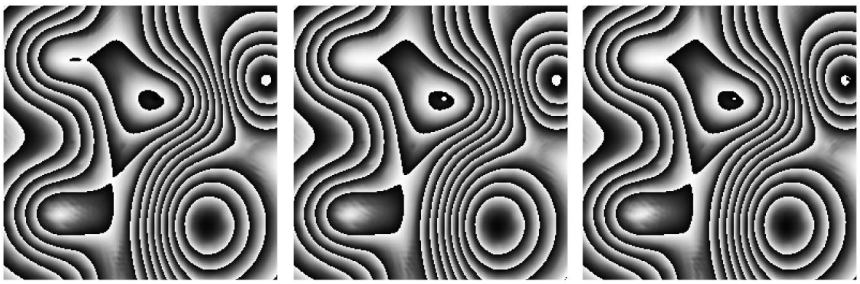

(a) (b) (c)

Fig. 7. Filtered results of Fig. 6. (a) Filtered phase obtained using β_T; (b) filtered phase obtained using β_{WFR}; (c) filtered phase obtained using β_{GRA}.

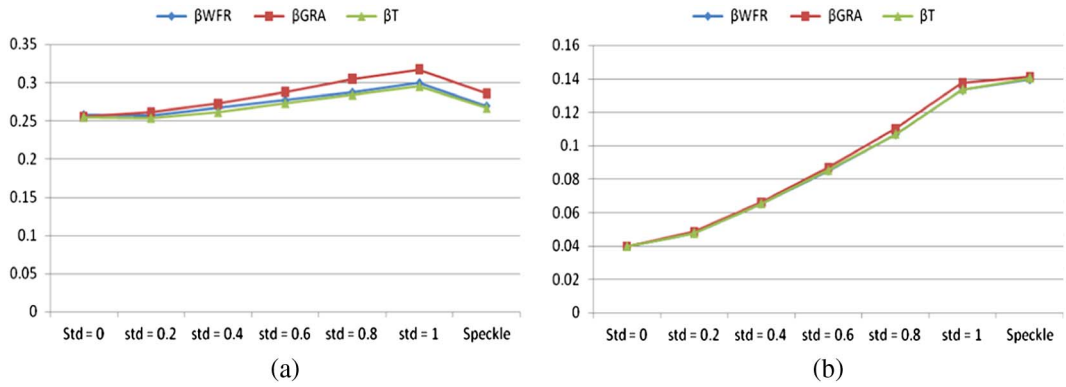

(a) (b)

Fig. 8. (Color online) Demodulation error plots. (a) Error plots of demodulation results in low density regions; (b) error plots of demodulation results in high density regions.

the ground-truth, while those for the experimental fringe pattern are qualitatively compared. The obtained directions will be further used in SPQ-transform for fringe demodulation [7,8].

A. Simulated Fringe Pattern

A fringe pattern is simulated and shown in Fig. 2(a), with a size of 256×256, fringe amplitude of 1, wrapped phase and theoretical direction β_T shown in Fig. 2(b) and 2(c), respectively. Additive noise with mean of zero and standard deviation (STD) of 0.2, 0.4, 0.6, 0.8, or 1.0 is simulated into the fringe pattern. Speckle noise with speckle size of 1 pixel is also simulated and it is shown in Fig. 2(d). For the WFR-based technique, the exhaustive searching range of ξ and η is set to $[-1.5, 1.5] \times [0, 1.5]$; the frequency step is 0.025; the window size along x and y axis of the windowed Fourier element is 4. Gaussian filterers are used to smooth the WFR results, with $\sigma_L = 6$ and $\sigma_H = 4$. For the gradient-based technique, $\sigma = 1.5$ and $\rho = 5$ are used.

For fringe pattern in Fig. 2(d), the WFR gives the orientation θ_{WFR} and density (quality) D_{WFR} in Figs. 3(a) and 3(b), respectively, based on which the quality-guided orientation unwrapping gives the direction β_{WFR} in Fig. 3(c). Some stripes are observed in Fig. 3(b), which is due to the small window size used in the WFR, but it does not affect the orientation unwrapping. Similarly, the gradient-based

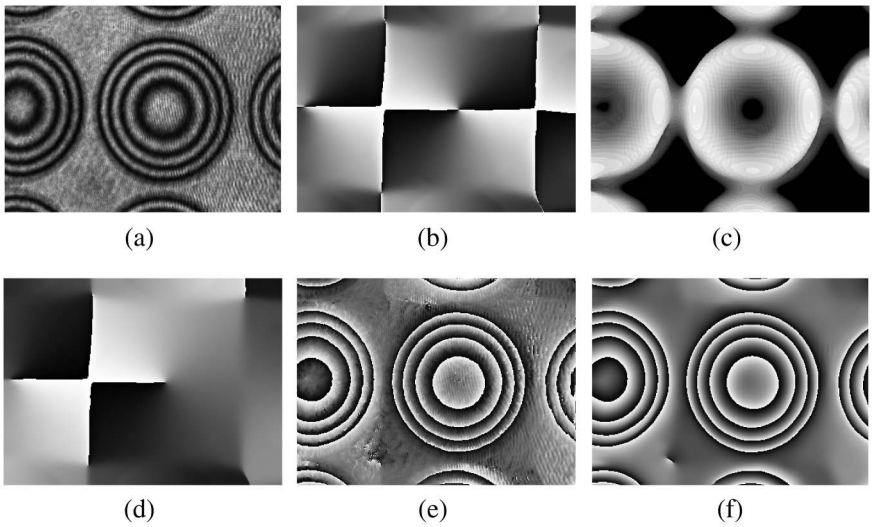

Fig. 9. Direction and phase obtained with WFR-based orientation unwrapping. (a) An experimental fringe pattern (image courtesy: Weijuan Qu, Ngee Ann Polytechnic); (b) orientation θ_{WFR}; (c) density D_{WFR}; (d) direction β_{WFR}; (e) phase obtained using β_{WFR}; (f) filtered phase of (e).

technique gives orientation θ_{GRA} in Fig. 4(a), density (quality) D_{GRA} in Fig. 4(b), and the unwrapped orientation, i.e., direction β_{GRA}, in Fig. 4(c). Both results are satisfactory. To measure the results quantitatively, direction error is calculated as

$$E_\beta = \frac{\sum_{y=1}^{N}\sum_{x=1}^{M}\left|2\sin\left[\frac{\beta(x,y)-\beta_T(x,y)}{2}\right]\right|}{M\times N}, \qquad (16)$$

where β is the estimated direction and $M \times N$ is the size of the fringe pattern. As mentioned earlier, the WFR has lower accuracy for local frequency estimation in low frequency regions comparing with high frequency regions. Thus the direction errors are evaluated for low and high frequency regions separately, identified with a threshold value of $\omega_{\mathrm{TLF}}(x,y) = 0.1$, to reveal more details. Plots of direction errors with respect to the noise levels are shown in Fig. 5. It can be seen that β_{WFR} is preferred if the fringe pattern is noisy (STD > 0.4); otherwise β_{GRA} can be used. The computation is carried out using MATLAB programming in an Intel Xeonquad-core CPUs of 2.5 GHz main frequency computer. The time costs for β_{WFR} and β_{GRA} are 260 s and 3 s, respectively. The gradient-based orientation unwrapping is much faster as is expected. The speed of the WFR-based orientation unwrapping can be accelerated by parallel computing [28].

The directions obtained by the two proposed techniques, β_{WFR} and β_{GRA}, are then used in the SPQ-transform based demodulation technique [7,8]. The

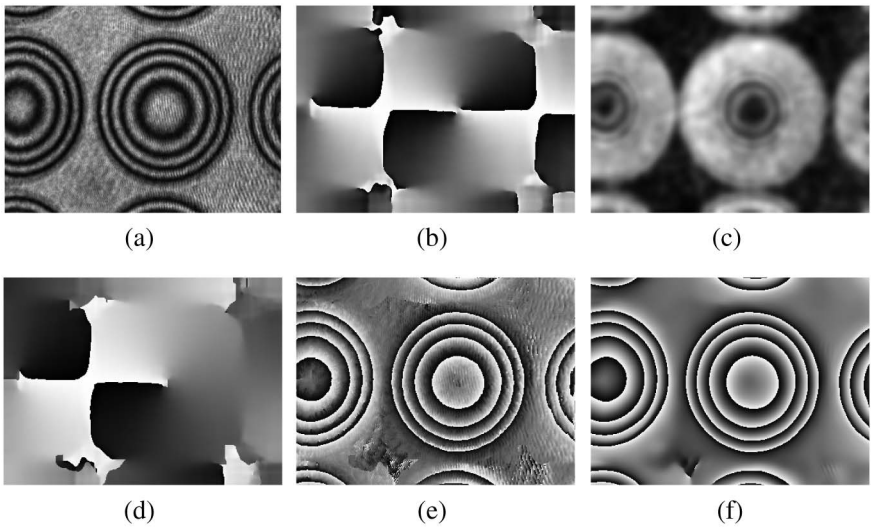

Fig. 10. Direction and phase obtained with gradient-based orientation unwrapping. (a) Experimental fringe pattern; (b) orientation θ_{GRA}; (c) density D_{GRA}; (d) direction β_{GRA}; (e) phase obtained using β_{GRA}; (f) filtered phase of (e).

phase results of Fig. 2(d) using β_T, β_{WFR}, and β_{GRA} are shown in Fig. 6. They are further denoised using the windowed Fourier filtering technique [21,22] and the results are shown in Fig. 7. Phase errors are measured using Eq. (16), with β and β_T replaced by the demodulated phase and ideal phase, respectively. They are plotted in Fig. 8 based on low and high density regions, respectively. From Figs. 6 to 8, it can be seen that both β_{WFR} and β_{GRA} help to successfully demodulate the phase from a single closed fringe pattern and the results are very close to the phase obtained using theoretical direction β_T.

B. Experimental Fringe Pattern

An experimental fringe pattern with size of 288×384 is shown in Fig. 9(a) to validate the conclusion drawn for simulated fringe patterns. It is captured from an in-line configuration of the digital holography system [29] for microlens characterization. For the WFR-based orientation unwrapping, the exhaustive searching range of ξ and η for the WFR is set to $[-1.5, 1.5] \times [0, 1.5]$; the frequency step and the window size are 0.025 and 10, respectively; the kernel sizes of Gaussian filter are $\sigma_L = 15$ and $\sigma_H = 4$. For the gradient-based technique, $\sigma = 1.5$ and $\rho = 5$. The WFR-based orientation θ_{WFR}, density D_{WFR}, and direction β_{WFR} are shown in Figs. 9(b)–(d), respectively. The direction β_{WFR} is then used in the SPQ based demodulation technique. The demodulation result is shown in Fig. 9(e), which is further filtered by windowed Fourier filtering and shown in Fig. 9(f). The original fringe pattern, the gradient-based orientation θ_{GRA}, density D_{GRA}, direction β_{GRA}, the phase result using β_{GRA}, and the filtered phase are shown in Fig. 10. The original fringe pattern in Fig. 10(a) is replicated from Fig. 9(a) for easier comparison between Fig. 9 and Fig. 10. It can be seen that, the performances of β_{WFR} and β_{GRA} are consistent with the simulated fringe patterns. The two proposed techniques are considered effective in processing experimental fringe pattern.

6. Conclusion

A quality-guided orientation unwrapping scheme is proposed to estimate the direction from orientation. Following the unwrapping scheme, a WFR-based orientation unwrapping technique and a gradient-based orientation unwrapping technique are proposed. The first technique estimates the orientation and density map using the WFR while the second technique uses existing orientation and estimates the density map from the gradient information. The WFR-based orientation unwrapping technique provides directions with high accuracy at a cost of long computing time. The gradient-based orientation unwrapping technique is also able to achieve accurate direction but is much faster. The modulo 2π directions of the proposed techniques are applied to the SPQ-transform based demodulation technique with good results. The two proposed techniques are thus considered effective and can be used as alternatives to each other.

References

1. D. W. Robinson and G. T. Reid, eds., in *Interferogram Analysis: Digital Fringe Pattern Measurement Techniques* (Institute of Physics, 1993).
2. Q. Yu, X. Sun, X. Liu, and Z. Qiu, "Spin filtering with curve windows for interferometric fringe patterns," Appl. Opt. **41**, 2650–2654 (2002).
3. C. Tang, L. Han, H. Ren, D. Zhou, Y. Chang, X. Wang, and X. Cui, "Second-order oriented partial-differential equations for denoising in electronic-speckle-pattern interferometry fringes," Opt. Lett. **33**, 2179–2181 (2008).
4. H. Wang, Q. Kemao, W. Gao, S. H. Soon, and F. Lin, "Fringe pattern denoising using coherence enhancing diffusion," Opt. Lett. **34**, 1141–1143 (2009).
5. J. Villa, J. A. Quiroga, and I. Rosa, "Regularized quadratic cost function for oriented fringe-pattern filtering," Opt. Lett. **34**, 1741–1743 (2009).
6. J. L. Marroquin, R. Rodriquez-Vera, and M. Servin, "Local phase from local orientation by solution of a sequence of linear system," J. Opt. Soc. Am. A **15**, 1536–1544 (1998).
7. K. G. Larkin, D. J. Bone, and M. A. Oldfield, "Natural demodulation of two-dimensional fringe patterns: I. general background of the spiral phase quadrature transform," J. Opt. Soc. Am. A **18**, 1862–1870 (2001).
8. M. Servin, J. A. Quiroga, and J. L. Marroquin, "General n-dimensional quadrature transform and its application to interferogram demodulation," J. Opt. Soc. Am. A **20**, 925–934 (2003).
9. J. A. Quiroga, D. Crespo, J. A. G. Pedrero, and J. C. Martinez-Antón, "Recent advances in automatic demodulation of single fringe patterns," FRINGE 2005 **1**, 90–97 (2006).
10. A. M. Siddiolo and L. D' Acquisto, "A direction/orientation-based method for shape measurement by shadow Moire," IEEE Trans. Instrum. Meas. **57**, 843–849 (2008).
11. X. Zhou, J. P. Baird, and J. F. Arnold, "Fringe-orientation estimation by use of a Gaussian gradient filter and neighboring-direction averaging," Appl. Opt. **38**, 795–804 (1999).
12. B. Jahne, *Practical Handbook on Image Processing for Scientific Applications* (CRC, 1997).
13. X. Yang, Q. Yu, and S. Fu, "A combined technique for obtaining fringe orientations of ESPI," Opt. Commun. **273**, 60–66 (2007).
14. K. G. Larkin, "Uniform estimation of orientation using local and nonlocal 2D energy operators," Opt. Express **13**, 8097–8121 (2005).
15. X. Yang, Q. Yu, and S. Fu, "An algorithm for estimating both fringe orientation and fringe density," Opt. Commun. **274**, 286–292 (2007).
16. C. Tang, Z. Wang, L. Wang, J. Wu, T. Gao, and S. Yan, "Estimation of fringe orientation for optical fringe patterns with poor quality based on Fourier transform," Appl. Opt. **49**, 554–561 (2010).
17. J. A. Quiroga, M. Servin, and F. Cuevas, "Modulo 2π fringe orientation angle estimation by phase unwrapping with a regularized phase tracking algorithm," J. Opt. Soc. Am. A **19**, 1524–1531 (2002).
18. M. Servin, J. L. Marroquin, and F. J. Cuevas, "Fringe-follower regularized phase tracker for demodulation of closed-fringe interferograms," J. Opt. Soc. Am. A **18**, 689–695 (2001).
19. H. Wang and Q. Kemao, "Frequency guided methods for demodulation of a single fringe pattern," Opt. Express **17**, 15118–15127 (2009).
20. D. Ghiglia and M. D. Pritt, *Two-Dimensional Phase Unwrapping* (Wiley, 1998).
21. Q. Kemao, "Windowed Fourier transform for fringe pattern analysis," Appl. Opt. **43**, 2695–2702 (2004).
22. Q. Kemao, "Two-dimensional windowed Fourier transform for fringe pattern analysis: Principles, applications and

implementations," Opt. Lasers Eng. **45**, 304–317 (2007).
23. Q. Kemao and S. H. Soon, "Sequential demodulation of a single fringe pattern guided by local frequencies," Opt. Lett. **32**, 127–129 (2007).
24. E. Davies, *Machine Vision: Theory, Algorithms and Practicalities* (Academic, 1990).
25. T. Lindeberg, *Scale_Space Theory in Computer Vision* (Kluwer, 1994).
26. J. Weickert, "Coherence-enhancing diffusion filtering," Int. J. Comput. Vis. **31**, 111–127 (1999).
27. O. S. Dalmau-Cedeño, M. Rivera, and R. Legarda-Saenz, "Fast phase recovery from a single close-fringe pattern," J. Opt. Soc. Am. A **25**, 1361–1370 (2008).
28. W. Gao, N. T. H. Huyen, H. S. Loi, and Q. Kemao, "Real-time 2D parallel windowed Fourier transform for fringe pattern analysis using Graphics Processing Unit," Opt. Express **17**, 23147–23152 (2009).
29. W. Qu, O. C. Chee, Y. Yu, and A. Asundi, "Characterization and inspection of microlens array by single cube beam splitter microscopy," Appl. Opt. **50**, 886–890 (2011).